Dynamic Evidence for an Extended Subsite Structure of the Ligand Combining Site on Wheat Germ Agglutinin: Temperature-Jump Relaxation with Fluorescence Detection†

Robert M. Clegg,* Frank G. Loontiens,‡ Nathan Sharon,§ and Thomas M. Jovin

ABSTRACT: Temperature-jump relaxation methods have been used to study the binding kinetics of fluorescent 4-methylumbelliferyl glycosides of *N*-acetyl-β-D-glucosamine and its β(1→4)-linked di- and trisaccharides with wheat germ agglutinin. The mono- and disaccharide derivatives yielded biexponential progress curves. The data are consistent with two simple mechanisms in which binding occurs to an extended combining site on the lectin, consisting of at least two different, mutually exclusive, binding subsites. For one model, the bound ligand must slide from one subsite to the other, and the other mechanism requires the dissociation of the bound ligand from the protein before it can combine to the other subsite. Binding of 4-methylumbelliferyl monosaccharide to nonequivalent sites is improbable. The underlying kinetic and equilibrium parameters were obtained for the proposed subsites. The binding kinetics of the 4-methylumbelliferyl trisaccharide derivative are more complicated and may result from ligand-mediated linking reactions between molecules of the lectin. This study emphasizes that binding studies at equilibrium should take into account that the data result from an average of different binding configurations of all the ligands.

Wheat germ agglutinin (WGA), a plant lectin (Lis & Sharon, 1977), binds specifically to 2-acetamido-2-deoxy-D-glucose (GlcNAc)[1] and its β(1→4)-linked oligosaccharides [$(GlcNAc)_n$] (Burger & Goldberg, 1967; Nagata & Burger, 1974; Allen et al., 1973; Privat et al., 1974c; Lotan & Sharon, 1973) and also to *N*-acetylneuraminic acid (Wright, 1980). The WGA molecule, M_r 36 000, is composed of two similar polypeptide chains and has two binding sites for neutral sugars per protomer, or four equivalent sites per M_r of 36 000 (Nagata & Burger, 1974; Privat et al., 1974a,b; Van Landschoot et al., 1977). It has been proposed that each binding site is composed of an extended region such that more than one monosaccharide unit of an oligosaccharide can interact simultaneously at each site. This concept was proposed to rationalize the observation that the association constants increase for the $(GlcNAc)_n$ series as the number of GlcNAc residues increases, as found by inhibition of agglutination reactions (Allen et al., 1973) and by titration experiments utilizing the increase in protein fluorescence upon ligand binding (Lotan & Sharon, 1973; Privat et al., 1974c). The subsite structure of the binding region is consistent with X-ray diffraction data obtained with $(GlcNAc)_2$ as a ligand (Wright, 1980). In contrast to the published equilibrium data, the work of Wright (1980) indicated two types of nonequivalent sites.

The fluorescent 4-methylumbelliferyl glycosides of per-*N*-acetyl chitooligosaccharides, $MeUmb(GlcNAc)_n$, have excellent optical properties for investigating the details of the protein–ligand interactions, since the fluorescence is largely quenched by binding to WGA (Privat et al., 1974b; Van Landschoot et al., 1977). The changes in the absorption of the MeUmb group upon binding to WGA also depend upon the carbohydrate chain length (Van Landschoot et al., 1977). The affinity of these compounds for WGA also depends upon the chain length, as originally proposed in the preliminary measurements of this study (Clegg et al., 1976), and this has been corroborated by extensive equilibrium measurements (Van Landschoot et al., 1977). Earlier results of Privat et al. (1974b) are inconsistent with both our kinetic and equilibrium measurements.

We present the results of temperature-jump experiments describing the kinetic processes involved when the ligands, $MeUmb(GlcNAc)_n$ (n = 1, 2, 3), bind to WGA. The multiple relaxations observed are interpreted in terms of models in which multiple subsites are within each binding region. It is possible, within the context of these models, to assign kinetic and equilibrium parameters to the separate subsites of the extended binding region of WGA, for the different binding configurations of the ligands, $MeUmb(GlcNAc)_n$ (n = 1, 2). The situation for $MeUmb(GlcNAc)_3$ is more complex. This study corroborates the proposals of an extended combining site and provides a kinetically mapped scheme for the subsite structure that is quantitatively analyzed. A preliminary report of this work has been published (Clegg et al., 1980).

Materials and Methods

$MeUmb(GlcNAcp)_n$, with n = 1, 2, and 3, were prepared as reported and their solutions were free from any contaminating 7-hydroxy-4-methylcoumarin (Delmotte et al., 1975; Van Landschoot et al., 1977). Wheat germ agglutinin (WGA) was prepared by affinity chromatography on Sepharose–2-acetamido-*N*-(ε-aminocaproyl)-2-deoxy-β-D-glucopyranosylamide (Lotan & Sharon, 1973); any activity of β-*N*-acetylglucosaminidase (2-acetamido-2-deoxy-β-D-glucoside acetamidodeoxyglucohydrolase, EC 3.2.1.30) was not detectable in samples of WGA as checked spectrofluorometrically (exitation 330 nm, emission 440 nm) with 0.5 mg/mL protein, 20 μM MeUmb-GlcNAc*p* as a substrate, and 10–20 min

† From the Abteilung Molekulare Biologie, Max-Planck-Institut für Biophysikalische Chemie, D-34 Göttingen, West Germany. *Received February 23, 1983.*

‡ Recipient of an EMBO fellowship. Laboratory of Biochemistry, Faculty of Science, State University of Gent, B-9000 Gent, Belgium.

§ Department of Biophysics, Weizmann Institute of Science, Rehovot, Israel.

[1] Abbreviations: WGA, wheat germ agglutinin; GlcNAc, 2-acetamido-2-deoxy-D-glucose; $(GlcNAc)_2$, *N*,*N*′-diacetylchitobiose; $(GlcNAc)_3$, *N*,*N*′,*N*″-triacetylchitotriose; $(GlcNAc)_4$, *N*,*N*′,*N*″,*N*‴-tetraacetylchitotetraose; MeUmb-GlcNAc, 4-methylumbelliferyl *N*-acetyl-β-D-glucopyranoside; $MeUmb(GlcNAc)_2$, 4-methylumbelliferyl *N*,*N*′-diacetylchitobioside; $MeUmb(GlcNAc)_3$, 4-methylumbelliferyl *N*,*N*′,*N*″-triacetylchitotrioside; CD, circular dichroism.

0006-2960/83/0422-4797$01.50/0

Table I: Kinetic and Thermodynamic Binding Parameters[a]

Parallel Model				Series Model			
$P + L \underset{k_{-1}^p}{\overset{k_1^p}{\rightleftharpoons}} C_1$ $\quad P + L \underset{k_{-2}^p}{\overset{k_2^p}{\rightleftharpoons}} C_2$				$P + L \underset{k_{-1}^s}{\overset{k_1^s}{\rightleftharpoons}} C_1 \underset{k_{-2}^s}{\overset{k_2^s}{\rightleftharpoons}} C_2$			
MeUmb-GlcNAc				MeUmb-GlcNAc			
$k_1^p = 1.5 \times 10^6$	$k_{-1}^p = 320$	$k_2^p = 1.5 \times 10^6$	$k_{-2}^p = 39$	$k_1^s = 3.0 \times 10^6$	$k_{-1}^s = 180$	$k_2^s = 110$	$k_{-2}^s = 69$
$K_1^p = 4.69 \times 10^3$	$\Delta H^\circ{}_1^p = -41.4$	$K_2^p = 3.85 \times 10^4$	$\Delta H^\circ{}_2^p = -34.5$	$K_1^s = 1.67 \times 10^4$	$\Delta H^\circ{}_1^s = -39.1$	$K_2^s = 1.6$	$\Delta H^\circ{}_2^s = 6.9$
$K_{tot}^p = 4.3 \times 10^4$	$\Delta H^\circ{}_{tot}^p = -35$			$K_{tot}^s = 4.3 \times 10^4$	$\Delta H^\circ{}_{tot}^s = -35$		
MeUmb(GlcNAc)$_2$				MeUmb(GlcNAc)$_2$			
$k_1^p = 9.3 \times 10^5$	$k_{-1}^p = 230$	$k_2^p = 1.1 \times 10^6$	$k_{-2}^p = 16$	$k_1^s = 1.0 \times 10^7$	$k_{-1}^s = 200$	$k_2^s = 21$	$k_{-2}^s = 18$
$K_1^p = 4.04 \times 10^4$	$\Delta H^\circ{}_1^p = -31.8$	$K_2^p = 6.88 \times 10^4$	$\Delta H^\circ{}_2^p = -38.6$	$K_1^s = 5 \times 10^4$	$\Delta H^\circ{}_1^s = -33$	$K_2^s = 1.2$	$\Delta H^\circ{}_2^s = -6.6$
$K_{tot}^p = 1.1 \times 10^5$	$\Delta H^\circ{}_{tot}^p = -36$			$K_{tot}^s = 1.1 \times 10^5$	$\Delta H^\circ{}_{tot}^s = -37$		

[a] Superscripts s and p refer to the series and parallel models, respectively. The units of the parameters are M^{-1} s^{-1} for k_j, s^{-1} for k_{-j}, M^{-1} for K_j, and kJ M^{-1} for ΔH° for all j's. The following defines the parameters in the table. $K_j = k_j/k_{-j}$, $K_{tot}^s = K_1^s(1 + K_2^s)$, $K_{tot}^p = K_1^p + K_2^p$, $\Delta H^\circ{}_{tot}^s = \Delta H^\circ{}_1^s + [K_2^s/(1 + K_2^s)]\Delta H^\circ{}_2^s$, $\Delta H^\circ{}_{tot}^p = (\Delta H^\circ{}_1^p K_1 + \Delta H^\circ{}_2^p K_2)/(K_1^p + K_2^p)$. The kinetically determined values $K_{tot}^s = K_{tot}^p$ compare favorably with the values 2.2×10^4 M^{-1} for MeUmb-GlcNAc and 8.4×10^4 M^{-1} for MeUmb(GlcNAc)$_2$ at 23.2 °C as calculated from the data of Van Landschoot et al. (1977).

incubation at 25 °C. Concentrations of WGA were determined spectrophotometrically with an absorption coefficient of 1.27 mg^{-1} cm^2 at 280 nm and were expressed on the basis of the equivalent mass of 9000, corresponding to two carbohydrate binding sites per subunit of M_r 18 000 (Rice & Etzler, 1975; Nagata & Burger, 1974; Privat et al., 1974a; Van Landschoot et al., 1977). Ligands and protein were dissolved in 0.1 M NaOAc/HOAc and 0.5 M NaCl, pH 4.7.

The temperature-jump apparatus has been described (Rigler et al., 1974). Ligand fluorescence was excited at 313 nm, and emission was measured above 360 nm through a cutoff filter. The temperature was increased by 3.2 °C to a final temperature of 23.2 °C. All experiments were performed as kinetic titration series with a varying concentration of WGA that was always in excess of a fixed concentration of ligand (2 μM). The free concentrations of ligand, $\bar{L}$, and protein, $\bar{P}$, were calculated from the appropriate equilibrium association constants determined by Van Landschoot et al. (1977).

The signal changes were digitized and stored in an on-line minicomputer (DEC PDP 11/20); the amplitudes and times of the relaxation curves were obtained with a nonlinear iterative procedure for fitting multiexponential decays of the signal (L. Avery, unpublished results). Exact simulations of the kinetic models, amplitudes, and times were done with a computer program written by L. Avery [unpublished results and Avery (1982)].

Results

The two ligands, MeUmb(GlcNAc)$_n$, with n = 1 and 2, show similar kinetic behavior. MeUmb(GlcNAc)$_3$ gives markedly different results, producing more relaxation processes and showing a concentration dependence of the relaxation parameters that is also qualitatively different from that for the other two ligands. We first present the data for MeUmb-GlcNAc and MeUmb(GlcNAc)$_2$, proposing two models that are consistent with the results. Then, we consider the kinetics for MeUmb(GlcNAc)$_3$, emphasizing the differences with the former two ligands.

MeUmb-GlcNAc and MeUmb(GlcNAc)$_2$. Both ligands form complexes with WGA such that the fluorescence of the MeUmb group is completely quenched (Privat et al., 1974b; Van Landschoot et al., 1977). The temperature-jump experiments were done as kinetic titrations, keeping the concentration of the ligands constant and varying the concentration of protein. Figure 1 is an example of a kinetic progress curve following a temperature jump of 3.2 °C, and Figures 2 and 3 are plots of the inverse relaxation times and the corresponding amplitudes as functions of the protein concentration. Two relaxation processes are observed throughout the concentration ranges with both ligands, and the dependencies of the relaxation times upon the concentration of the protein are similar. In each case, the inverse of the faster relaxation time increases linearly with increasing protein concentration, and the same plot for the slower relaxation indicates a plateau value after an initial increase. This type of behavior is indicative of two well-known two-step molecular mechanisms, the serial and parallel models defined in Table I. These two models are nearly indistinguishable (Viale, 1971), and since they are two of the simplest models displaying this behavior of the kinetic times and amplitudes, we will analyze the data in terms of them. Further consideration of these models is given under Discussion.

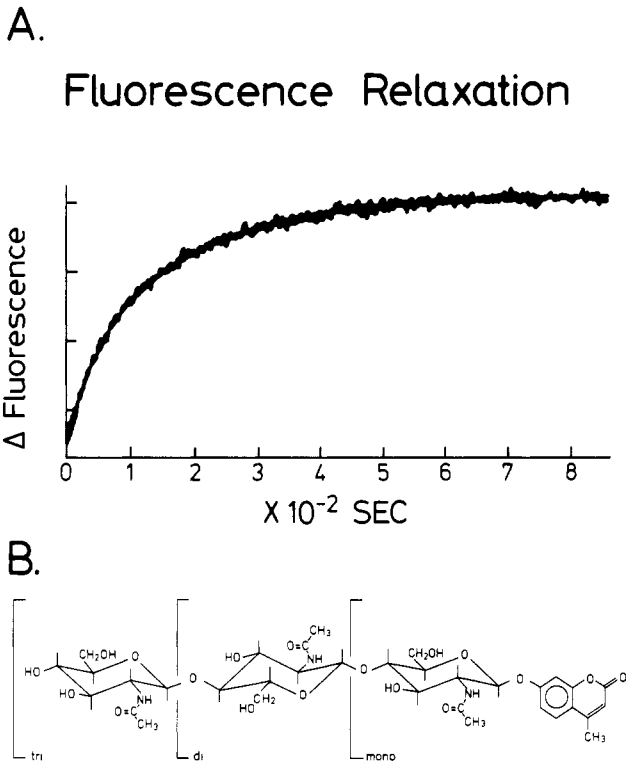

FIGURE 1: (A) Example of a temperature-jump experiment obtained from a solution containing 14.2 μM WGA binding sites and 2.1 μM MeUmb-GlcNAc. Two relaxation processes are required to fit the progress curve (τ_1 = 3.1 ms, τ_2 = 17.4 ms). (B) Chemical formula for MeUmb(GlcNAcp)$_n$, for n = 1, 2, and 3, the mono-, di-, and trisaccharide derivatives used as ligands.

Table II: Relaxation Time and Amplitude Expressions[a]

exptl parameters	parallel model	series model
$\tau_1^{-1} + \tau_2^{-1}$	$(k_1^{p} + k_2^{p})(\bar{P} + \bar{L}) + k_{-1}^{p} + k_{-2}^{p}$	$k_1^{s}(\bar{P} + \bar{L}) + k_{-1}^{s} + k_2^{s} + k_{-2}^{s}$
$\tau_1^{-1}\tau_2^{-1}$	$(k_1^{p}k_{-2}^{p} + k_2^{p}k_{-1}^{p})(\bar{P} + \bar{L}) + k_{-1}^{p}k_{-2}^{p}$	$k_1^{s}(k_2^{s} + k_{-2}^{s})(\bar{P} + \bar{L}) + k_{-1}^{s}k_{-2}^{s}$
$\Delta P_1/(P_O - P_M)$	$(\Delta \ln K_1^{p})[k_{-1}^{p}/(1 + K_2^{p}/K_1^{p})]\tau_1$	$(\Delta \ln K_1^{s})[k_{-1}^{s}/(1 + K_2^{s})]\tau_1$
$\Delta P_2/(P_O - P_M)$	$(\Delta P_{tot} - \Delta P_1)/(P_O - P_M)$	$(\Delta P_{tot} - \Delta P_1)/(P_O - P_M)$
$\Delta P_{tot}/(P_O - P_M)$	$k_{-1}^{p}k_{-2}^{p}[(\Delta \ln K_1^{p})K_1^{p} + (\Delta \ln K_2^{p})K_2^{p}]\tau_1\tau_2/(K_1^{p} + K_1^{p})$	$k_{-1}^{s}k_{-2}^{s}[\Delta \ln K_1^{s} + (\Delta \ln K_2^{s})K_2^{s}/(1 + K_2^{s})]\tau_1\tau_2$

[a] Expressions for the sum and product of the two relaxation times (τ_1 and τ_2), the relative amplitudes for the faster (ΔP_1) and slower (ΔP_2) relaxation, and the total amplitude ($\Delta P_{tot} = \Delta P_1 + \Delta P_2$). The expressions for the times are general, but the formulas for the relative amplitudes assume that the relaxation processes are well separated in time. The symbols are as defined for the models in Table I. ΔP_i refers to the observed kinetic amplitude for the ith relaxation process. P_O is the static fluorescence in the T-jump cell that would be observed provided that there were no binding (including fluorescence from the protein), and P_M is the measured static fluorescence.

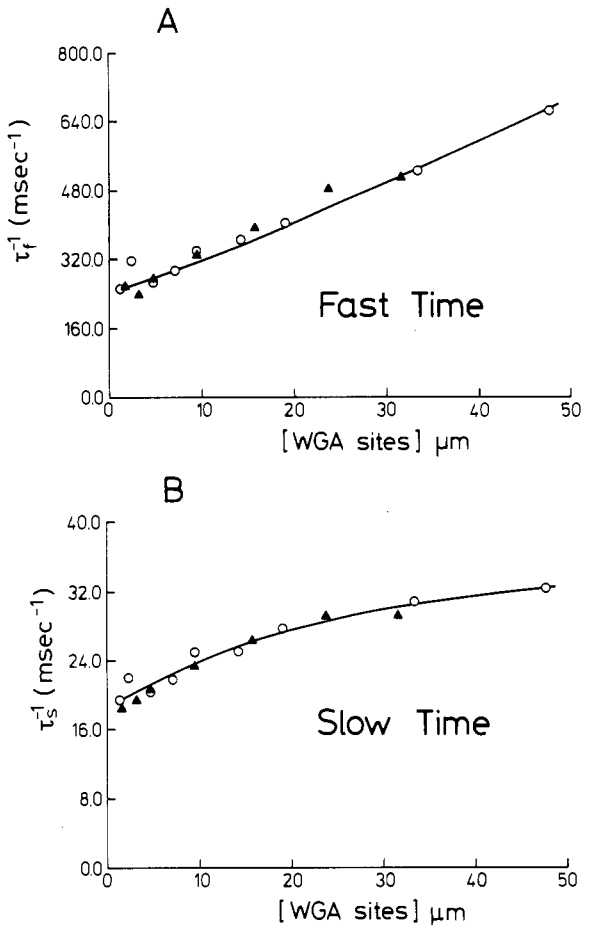

FIGURE 2: Results of the relaxations for two independent series of relaxation experiments are presented (▲ and ○) for solutions of WGA and MeUmb(GlcNAc)$_2$. The concentration of ligand was kept constant for each series at about 2 μM. The x axis is the total concentration of the binding sites (two per protomer) of WGA, and the y axis is the inverse of the fast or slow relaxation time in milliseconds^{-1}. The solid line is the exact simulation of the data for the parallel model from the parameters of Table I, simultaneously considering the times and amplitude of both relaxation processes (see text).

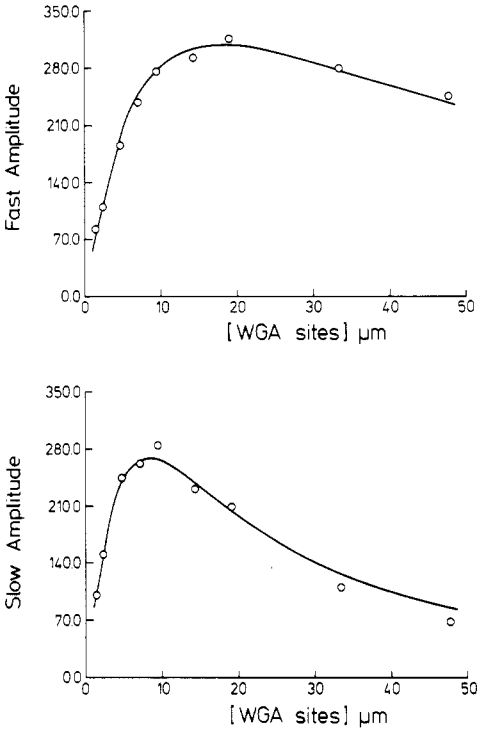

FIGURE 3: Relaxation amplitude data corresponding to one of the time series of Figure 2. The comments in the legend for Figure 2 apply. The y axis for both plots is the measured amplitude in arbitrary, but comparable, units.

Table I lists the parameters derived for each model. These two models are characterized by indistinguishable concentration dependence of the relaxation times, and they can be distinguished only from the behavior of the amplitudes under special conditions (Viale, 1971), which we cannot achieve experimentally. A simple method to determine the rate constants of both models is to determine the slopes and intercepts for plots of the sum and the product of the inverse relaxation times vs. the free concentration of reactants (Table II). The change in enthalpy for each step of the mechanisms is derived from the concentration dependence of the kinetic amplitude data. If the relaxation times are sufficiently separated, as they are for MeUmb(GlcNAc)$_2$, the following simple method can be used. The equations of Table II may be derived by using the assumption of separated times (see Appendix). Thus, by plotting the relative amplitude, $\Delta P_1/(P_O - P_M)$ (Table II), of the fast process vs. the corresponding relaxation time, τ_1, we can calculate ΔH°_1 (enthalpy change for step 1) for either model from the slope, since we know k_1 and k_{-1} independently from the analysis of the times. Then, we plot the relative total amplitude, $\Delta P_{tot}/(P_O - P_M)$, vs. the product of the two relaxation times, and the resulting slope can be used to calculate the enthalpy change for the second step (ΔH°_2) since we know ΔH°_1 and all the reaction rate constants. Figure 4 represents such plots for MeUmb(GlcNAc)$_2$, and the derived ΔH° values are given in Figure 4. This analysis is straightforward and gives reliable results without a nonlinear regression analysis of the amplitudes as a function of the concentration. It is also evident that both models predict the same behavior, and under the assumptions of separated relaxation times, the two models cannot be distinguished on the basis of the amplitudes.

For MeUmb-GlcNAc, the relaxation times are not well enough separated to allow the above simplified analysis of the

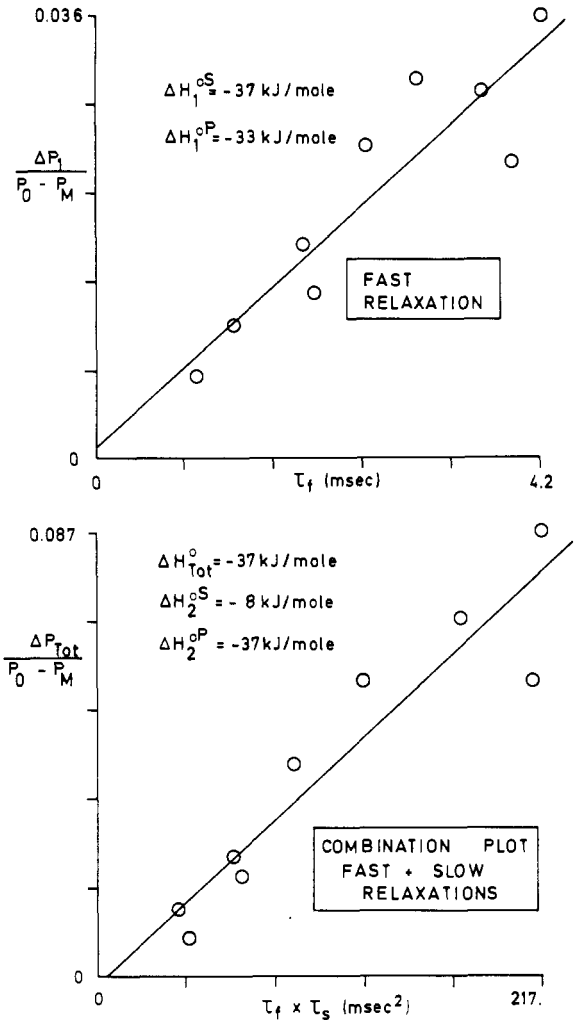

FIGURE 4: Plots of relative amplitudes as described and explained in Table II, the text, and the Appendix. The data correspond to one of the series for the ligand MeUmb(GlcNAc)$_2$. The thermodynamic information given in the figure is derived from linear fits of the data, by using the equations of Table II (for comparison, the corresponding values in Table I are results of exact nonlinear simulations).

amplitudes as was done for MeUmb(GlcNAc)$_2$. We can however attempt the simplified analysis and then use the resulting parameters as starting values to simulate the real amplitudes with expressions that do not involve any approximations. The enthalpy changes given in Table I for MeUmb-GlcNac are derived in this way.

MeUmb(GlcNAc)$_3$. Figure 5 summarizes the course of three out of four relaxation processes observed for MeUmb-(GlcNAc)$_3$ throughout the protein concentration range of 1–150 μM. The concentration dependence of the relaxation spectrum differs markedly from that of the other two ligands above. The relaxation not depicted in Figure 5 appears rather suddenly and after reaching a maximum at a protein concentration of 60 μM decreases rapidly again as the protein concentration increases. The three relaxations represented in Figure 5 seem to behave qualitatively as expected for the series and parallel models (see Table I); however, these simple models cannot correspond quantitatively to the data for MeUmb-(GlcNAc)$_3$ as we now show. We arbitrarily label the relaxations as 1, 2, 3, and 4 in the order of increasing relaxation times. We consider first the plots of the inverse relaxation times. $1/\tau_1$ increases linearly with the concentration, and the amplitude disappears when the total concentration of protein sites, [WGA], is 10 μM. $1/\tau_2$ increases to an eventual plateau that is higher than the intercept value ([WGA] = 0) for $1/\tau_1$.

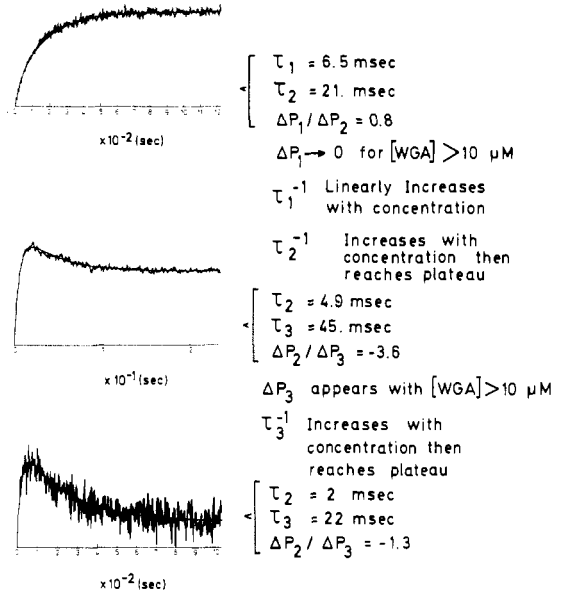

FIGURE 5: Representation of data for MeUmb(GlcNAc)$_3$ (44% apparent total quenching) indicating the approximate concentration at which the various effects are observed. The subscripts refer to the relaxation processes in the order of appearance. The general behavior of the relaxation spectrum as the concentration of WGA is varied, keeping the concentration of ligand constant, is as follows: (1) (First process) τ_1^{-1} increases with the concentration of WGA, and the amplitude decreases, becoming unobservable for [WGA] > 10 μM. The low concentration intercept is about 25 ms^{-1}. (2) (Second process) The plot of τ_2^{-1} vs. [WGA] is hyperbolic, the intercept is about 10 ms^{-1}, and the plateau value at high concentration WGA is 425 ms^{-1}. The amplitude decreases as the concentration of WGA increases after passing through a maximum at about 10 μM WGA. (3) (Third process) This process appears if [WGA] > 10 μM. The plot of τ_3^{-1} vs. [WGA] is hyperbolic; the low concentration intercept is about 1 ms^{-1}, and the high concentration plateau is 60–70 ms^{-1}. The amplitude passes through a maximum at 50 μM WGA and is still decreasing at the highest concentrations of WGA measured. (4) (Fourth process) This process (not shown) appears when the concentration of WGA is about 60 μM. See text.

This plateau value for $1/\tau_2$ is even higher than the highest $1/\tau_1$ value observed at about [WGA] = 10 μM. The plateau values for $1/\tau_2$ and $1/\tau_3$ are also higher than the intercept values ([WGA] = 0) of all the observed relaxations. It is important to notice that the plots for MeUmb-GlcNAc and MeUmb-(GlcNAc)$_2$ do not show this characteristic. That is, for them, the plateau of the inverse relaxation time of the slower relaxation is always less than the intercept value of the faster relaxation (see Figure 2).

It can be shown for the two models of Table I that the plateau value of $1/\tau$ for the slower relaxation can never be larger than the $1/\tau$ intercept of the faster relaxation and that this characteristic is generally true without any approximations of separated times (R. M. Clegg, unpublished results). This reasoning can be extended to series or parallel binding mechanisms with any number of steps; i.e., the plateau value of $1/\tau_n$ is always lower than the $1/\tau_{n-1}$ intercept, using the nomenclature for numbering the relaxations introduced above. Thus the concentration dependence for the relaxation times of MeUmb(GlcNAc)$_3$ differs radically from the behavior that is characteristic of the models in Table I. Therefore, in contrast to MeUmb-GlcNAc and MeUmb(GlcNAc)$_2$, additional equilibria must be involved in the complete description of the binding of MeUmb(GlcNAc)$_3$ to WGA. The equilibrium binding data for MeUmb(GlcNAc)$_3$ also show anomalies at higher concentrations of reactants (Van Landschoot et al., 1977), and the reactions underlying these anomalies may contribute to the relaxation spectrum (see Discussion).

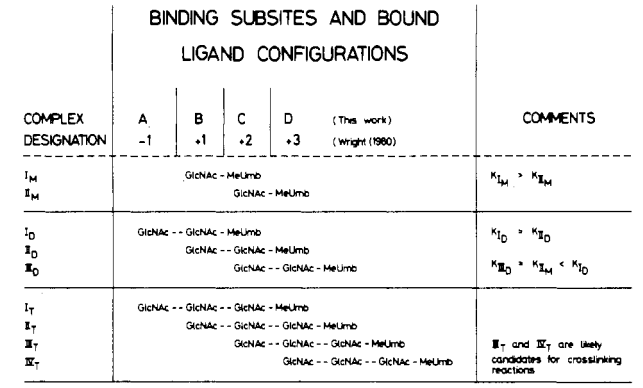

FIGURE 6: Subsites are considered to have the following characteristics: (Subsite A) Can accommodate a galactosyl residue (Wright, 1980; Bhavanandan & Katlic, 1979). (Subsite B) Specific for *N*-acetyl-D-glucosamine. (Subsite C) Specific affinity for *N*-acetyl-D-glucosamine; interacts with the aglycon, totally quenches the fluorescence of MeUmb, and has the main contribution in the difference absorption spectrum (Van Landschoot et al., 1977). (Subsite D) No pronounced interactions with carbohydrates, which are available to the solvent. This site also interacts the aglycon, quenches the MeUmb fluorescence, but has little effect on the MeUmb absorption. All groups positioned to the right of subsite D are free to interact with the solvent. The proposed relation of the binding affinities of the complexes is shown in the comments. The subscripts M, D, or T of the roman numerals refer to the mono-, di-, or trisaccharide, respectively. The *K*'s are association constants. The notation of Wright (1980) is given underneath the subsite designation at the top of the figure.

Discussion

Figure 6 illustrates a simple model with multiple subsites and the binding possibilities for the three MeUmb saccharide derivatives. Two neighboring subsites (B and C) are specific for *N*-acetyl-D-glucosamine, and a third subsite (D) interacts with the MeUmb aglycon. Such a linear array of the subsites accounts for the assumption, inherent in both reaction models of Table I, that all bound configurations are mutually exclusive. The models in Figure 6 and Table I include the possibility that ligands can form different complexes within a binding region, and the two relaxations observed with MeUmb-GlcNAc indicate that at least two GlcNAc-specific subsites are present. Multiple subsite interpretations from equilibrium measurements have not previously considered separate modes of binding to the extended binding region. The molecular details of the two mechanisms presented in Table I are different, even though both mechanisms predict an identical concentration dependence of the two relaxation times.

We first discuss the two models of Table I for the MeUmb-GlcNAc and MeUmb$(GlcNAc)_2$ ligands, after which we examine a third model involving nonequivalent binding regions on WGA, which we show to be unlikely. Then, we consider equilibrium and X-ray crystallographic data that can account for the complexity of the kinetics observed with MeUmb$(GlcNAc)_3$.

Parallel Model. The parallel model represents the association of a ligand to a binding region on the protein with multiple subsites, such that the formation of one bound configuration precludes further binding to the binding region. Each reaction involves a bimolecular binding association, requiring the complete dissociation of the ligand from the protein before the ligand can participate in a different complex. The ratio of any two equilibrium binding constants is equal to the ratio of the concentrations of the two corresponding bound configurations. Table I indicates that the affinity for one of the complexes with MeUmb-GlcNAc is much larger than that for the other. The two forward rate constants for MeUmb-GlcNAc are the same, indicating similar rate-controlling processes for the two binding possibilities. The dissociation rate constants account for the difference in the affinities of the two bound forms. In contrast, although the two dissociation rate constants for MeUmb$(GlcNAc)_2$ differ by 1 order of magnitude, the forward rate constants are also considerably different, resulting in two MeUmb$(GlcNAc)_2$ complexes with comparable affinity.

The models in Table I are sufficient to represent the observed relaxation spectrum for MeUmb-GlcNAc and MeUmb$(GlcNAc)_2$. However, neither of the models accounts for all the binding possibilities for MeUmb$(GlcNAc)_2$ shown in Figure 6. This requires another kinetic step to account for the third configuration, III_D. The fact that we cannot observe a third relaxation could be due to weak binding of MeUmb-$(GlcNAc)_2$ as complex III_D. It is possible that the complex III_D of MeUmb$(GlcNAc)_2$ is less stable than even the II_M complex for MeUmb-GlcNAc, since the MeUmb group does not add to the affinity of the III_D complex of Figure 6. This weakly bound state for MeUmb$(GlcNAc)_2$ would be very sparsely populated and would not contribute significantly to the relaxation spectrum. This accounts for the two relaxations for the disaccharide, even though the model of Figure 6 would predict three. The association constants of the other MeUmb$(GlcNAc)_2$ complexes (I_D and II_D) are only slightly larger than for the most stable complex I_M with MeUmb-GlcNAc (Table I), presumably because of the increase in the free energy of binding due to the MeUmb group in the complex I_M.

Series Model. The series model consists of a bimolecular binding step followed by a monomolecular change. The latter process is often attributed to a conformational change of the protein; however, any monomolecular rearrangement of the complex is possible. Our kinetic results are consistent with this model, and according to the scheme of Figure 6, we interpret the monomolecular step to be a sliding movement of the bound ligand among the subsites within the binding region. The reaction rate constants pertaining to the monomolecular step for the two ligands are quite different (Table I). This supports a sliding mechanism, since an induced conformational change involving rearrangements primarily in the protein structure of the complex would probably have similar monomolecular rate constants for different ligands. Thomas et al. (1977) attributed changes in the CD spectrum of WGA upon carbohydrate binding to local changes within the binding region and not to any overall rearrangement of the polypeptide chain. Thus the analysis of our results in terms of the series model also suggests an extended binding site on the protein consisting of multiple subsites. Similar considerations as for the parallel model rationalize why two, rather than three, relaxation processes are seen for MeUmb$(GlcNAc)_2$.

Unlikely Alternative Model with Nonequivalent Sites. A preliminary crystallographic study using MeUmb$(GlcNAc)_2$ as a ligand proposed that the combining sites were located between the intrapolypeptide domains (Wright, 1977); however, it was subsequently shown (Wright, 1980) that these locations were artifacts caused by a different amount of glutaraldehyde cross-linking in the crystals of WGA and of the WGA–MeUmb$(GlcNAc)_2$ complex. The latter data indicated two nonequivalent, though similar extended combining sites located at the promoter/promoter contact regions: a primary site that binds $(GlcNAc)_2$, as well as *N*-acetylneuraminic acid, and a secondary site that binds only $(GlcNAc)_2$ weakly. However, it is likely that cross-linking by glutaraldehyde slightly displaces $(GlcNAc)_2$ from its optimum binding position

at the secondary site (Wright, 1980). It should be stressed that the latter results contrast with all binding data in solution published to date that do not indicate any functional difference between the binding regions of WGA. We now explain why we do not consider two nonequivalent binding sites as an alternative model.

The kinetic data for MeUmb-GlcNAc and MeUmb-$(GlcNAc)_2$ can be satisfactorily accounted for by assuming two bimolecular kinetic steps at two nonequivalent and independent sites. However, the two apparent equilibrium constants determined kinetically for two assumed nonequivalent sites differ by a factor of 6 for MeUmb-GlcNAc. If the sites were nonequivalent, the equilibrium binding experiments (Privat et al., 1974b; Van Landschoot et al., 1977) would show nonlinear Scatchard plots, and the asymptotic linear fit at low site occupation would extrapolate to half the number of binding sites on the protein. This is definitely not observed. Equilibrium measurements with MeUmb-GlcNAc and MeUmb-$(GlcNAc)_2$ show linear Scatchard plots, and the number of equivalent sites corresponds to four in the dimeric molecule (Privat et al., 1974a,b; Van Landschoot et al., 1977).

Therefore, we do not consider this nonequivalent two-site model any further. We note that the apparent consistency of this model with the kinetic results is due only to the fact that the concentration of the protein was varied in the present experiments. The nonequivalent site model does not predict that the inverse time of the slow relaxation would reach a plateau value if the ligand concentration was varied. Unfortunately, fluorescence detection does not allow variation of the concentration of a ligand over a sufficiently large range to directly test this.

MeUmb$(GlcNAc)_3$. The observed concentration dependence of the four relaxation times for MeUmb$(GlcNAc)_3$ is incompatible with either the series or the parallel model, even if the models are extended for any number of similar kinetic steps [i.e., bimolecular associations for the parallel model or consecutive monomolecular reactions (slidings) for the series model]. Neither of these extended models permits the inverse of a slower relaxation time to cross the intercept value (at zero concentration of the reactants) of a faster process. Neighboring intercepts of the inverse relaxation times limit the allowed values of any relaxation time, and the relaxation time is never allowed to cross these boundaries, as the concentrations of the reactants are varied. This property of the normal modes is an exact result for both models and involves no approximations of the relaxation equations (R. M. Clegg, unpublished results). These conditions are not fulfilled for MeUmb-$(GlcNAc)_3$, and therefore, neither of the two models of Table I, extended to any number of steps, can represent the binding of MeUmb$(GlcNAc)_3$ to WGA.

Thus, we must propose additional reaction possibilities to account for the relaxation spectrum of MeUmb$(GlcNAc)_3$. Candidates for such processes include site–site interactions, nonequivalent combining sites, and aggregation reactions caused by cross-linking with MeUmb$(GlcNAc)_3$. There is no direct evidence for cooperative interactions between the sites of the dimer for MeUmb-GlcNAc or MeUmb$(GlcNAc)_2$ (Privat et al., 1974b; Van Landschoot et al., 1977) so we discard the first possibility. The other two possibilities should be considered in light of the following results. Anomalies are observed when WGA binds to concentrations of MeUmb-$(GlcNAc)_3$ (20 μM) that are higher than in the present study, and a precipitate is formed (Privat et al., 1974b; Van Landschoot et al., 1977). This is direct evidence of an interaction between the WGA dimers in solution caused by linking the WGA dimers by MeUmb$(GlcNAc)_3$. MeUmb-GlcNAc does not show this effect, even at near saturation of WGA; apparently, this monosaccharide derivative is too short to induce precipitation. In comparison to MeUmb$(GlcNAc)_3$, MeUmb$(GlcNAc)_2$ shows a similar behavior, though less pronounced and at higher concentrations.

When MeUmb$(GlcNAc)_3$ binds to WGA, it is impossible for its *N*-acetyl-D-glucosamine groups to interact at two binding regions of a single WGA dimer since its carbohydrate chain length is too short to span the minimum required distance (Wright, 1980). Since precipitation is not observed with $(GlcNAc)_3$ or $(GlcNAc)_4$, both of which dissolve the MeUmb$(GlcNAc)_3$–WGA complex, we assume that linking of WGA dimers by MeUmb$(GlcNAc)_3$ occurs due to the interaction of one WGA dimer with the MeUmb group of a MeUmb$(GlcNAc)_3$ ligand that is bound to another WGA dimer via the $(GlcNAc)_3$ moiety. This is suggested by the observation that per-*N*-acetyl chitooligosaccharides larger than $(GlcNAc)_2$ cannot bind to the glutaraldehyde-linked protein crystals. Model building indicates that $(GlcNAc)_3$ causes crowding at the primary site and completely blocks the secondary site (Wright, 1980). Thus the MeUmb group may be accessible to solvent or to another WGA molecule when MeUmb$(GlcNAc)_3$ is bound. In addition, it may be that the length or the conformation of MeUmb$(GlcNAc)_3$ is sufficient to probe any nonequivalence of the binding regions, in contrast to MeUmb-GlcNAc or MeUmb$(GlcNAc)_2$.

Multiple Binding Configurations at the Extended Binding Regions. The previously proposed schemes of interaction for $(GlcNAc)_n$ at an extended binding region composed of subsites have resulted from static measurements and have considered only one bound configuration for each of these ligands (Allen et al., 1973; Lotan & Sharon, 1973; Privat et al., 1974c). This is also true for the results obtained from a detailed equilibrium study on binding of MeUmb$(GlcNAc)_n$, resulting in a model by Van Landschoot et al. (1977) that was shown by Monsigny et al. (1978) to be compatible with the increase in fluorescence and phosphorescence of the protein, observed upon binding of 1-(thiomercuri)benzoate glycosides of per-*N*-acetyl chitooligosaccharides.

The present kinetic results corroborate the concept of an extended arrangement of subsites, and our data provide dynamic evidence consistent with the interchange of the bound ligands among the possible complex forms. The association constants corresponding to each individual binding mode of MeUmb-GlcNAc and MeUmb$(GlcNAc)_2$ with WGA can be derived from the kinetic experiments. On the basis of these kinetically determined binding parameters and the equilibrium evidence (Van Landschoot et al., 1977), we propose the schematic model of Figure 6 to represent the possibilities for the ligands to bind to the multiple subsite arrangement of WGA. The subsites B and C are assumed to bind GlcNAc groups almost equally well, and subsite A interacts only weakly, if at all, with *N*-acetyl-D-glucosamine. The protein surface to the right of subsite C is assumed not to interact specifically with the saccharides. The numbers below the subsites of Figure 6 refer to the labeling of Wright (1980). The MeUmb fluorescence is assumed to be totally quenched when contacting subsites C and D but not totally quenched when positioned to the right of D. At subsite C, the MeUmb group produces an intense difference absorption (Van Landschoot et al., 1977). The MeUmb group is also considered to interact with the protein to the right of, and including, subsite C. We have assigned the binding parameters to each complex of the proposed subsite structure according to the

following criteria, which the schematic model of Figure 6 fulfills.

(1) One binding configuration of MeUmb-GlcNAc (I_M in Figure 6) has additional interactions of the MeUmb group to the protein. The difference in affinities between the two bound forms is due to the reaction entropy, $\Delta S°$, and not $\Delta H°$. This is consistent with the assignment of the most affine complex with MeUmb-GlcNAc to the configuration shown as I_M in Figure 6. Formation of I_M would involve the removal of more ordered water molecules surrounding the MeUmb group, thereby increasing the overall entropy change and the stability of I_M. This is further substantiated by the difference absorption spectrum for MeUmb-GlcNAc (with I_M as the preferred complex) that is more intense than for MeUmb-$(GlcNAc)_2$ (Van Landschoot et al., 1977). Note the position of the MeUmb group for the complexes I_D and II_D in comparison to that of the complex I_M with comparable affinity. (2) The affinity of one binding mode of MeUmb-GlcNAc (II_M) approaches the weak binding of *N*-acetyl-D-glucosamine (Privat et al., 1974c; Lotan & Sharon, 1973), indicating only a weak contribution of MeUmb to the affinity for the II_M complex. (3) One binding mode of MeUmb-GlcNAc, I_M, has a stability equal to one mode of binding for MeUmb-$(GlcNAc)_2$, I_D, suggesting a negligible contribution by subsite A. (4) Two of the bound forms of MeUmb$(GlcNAc)_2$ have similar affinities. The ligand would interact much less strongly in the third form, III_D, and this complex would not be observable; the fluorescence of the MeUmb group is not quenched in this form. (5) Due to the interaction of the MeUmb group with the protein, particularly with the smaller ligands, the series of ligands MeUmb$(GlcNAc)_n$ as n increases from 1 to 3, does not show as large an increase in overall affinity for WGA as does the series of $(GlcNAc)_n$. (6) Multiple relaxation processes are expected, due to the multiple subsites. (7) At equilibrium with WGA, the spectroscopic observations with the umbelliferyl derivatives (Van Landschoot et al., 1977) and the (thiomercuri)benzoate derivatives (Monsigny et al., 1978) of per-*N*-acetyl chitooligosaccharides are consistent with this model. (8) Since in the oligosaccharides *N*-acetyl-D-glucosamine groups positioned to the right of subsite C are assumed not to interact with the protein and are accessible to the solvent, MeUmb$(GlcNAc)_2$ and MeUmb$(GlcNAc)_3$ could interact with two WGA dimers simultaneously, the trisaccharide more strongly than the disaccharide. Solutions of WGA and MeUmb$(GlcNAc)_3$ become turbid if the ratio of the ligand to protein is about 0.5 (Privat et al., 1974b; Van Landschoot et al., 1977). MeUmb$(GlcNAc)_2$ shows this behavior to a lesser extent (Van Landschoot et al., 1977). Precipitation is not observed with $(GlcNAc)_n$ under similar conditions. (9) The aggregation reactions proposed in (8) could participate in the relaxation spectrum for MeUmb$(GlcNAc)_3$ as the protein concentration increases. (10) The model is consistent with the crystallographic results of Wright (1980). The disaccharide $(GlcNAc)_2$ would be expected to have one strongly interacting mode according to the model, II_D as suggested by Wright (1980).

The extended binding region on WGA contrasts with the much simpler case for another well-studied lectin, concanavalin A. Extensive equilibrium (Loontiens et al., 1977a; Van Landschoot et al., 1978) and kinetic (Clegg et al., 1977, 1981; Loontiens et al., 1977b; Van Landschoot et al., 1980) studies with similar ligands, where the specific carbohydrate is α-D-mannopyranoside, have all indicated that the binding region on concanavalin A contains a single site that is specific for the carbohydrate. The kinetic rate constants of corresponding elementary reactions are greater for WGA by a factor of 10–100 than for concanavalin A. Whether these differences are significant for the biological interactions of the these two lectins remains to be seen. The multiple binding possibilities for *N*-acetyl-D-glucosamine groups within a binding site must be considered in order to interpret future spectroscopic and binding measurements with WGA.

Appendix

The equations in Table II are derived. The differential matrix equations describing the models of Table I are, for the parallel model

$$\frac{d}{dt}\Delta\epsilon^P = \begin{bmatrix} k_1^P(\bar{P}+\bar{L}) + k_{-1}^P & k_1^P(\bar{P}+\bar{L}) \\ k_2^P(\bar{P}+\bar{L}) & k_2^P(\bar{P}+\bar{L}) + k_{-2}^P \end{bmatrix} \Delta\epsilon^P \qquad \text{(A1)}$$

and for the series model

$$\frac{d}{dt}\Delta\epsilon^S = \begin{bmatrix} k_1^S(\bar{P}+\bar{L}) + k_{-1}^S & -k_{-1}^S \\ -k_2^S & k_2^S + k_{-2}^S \end{bmatrix} \Delta\epsilon^S \qquad \text{(A2)}$$

The $\Delta\epsilon$'s are the vectors of the deviations of the extents of reaction from the equilibrium values, and d/dt is the time derivative. The formalism of Castellan (1963) is used.

The sum and product of the two eigenvalues (inverse relaxation times) for both models (Table II) are simply the trace and the determinant, respectively, of the matrices of eq A1 and A2. The expressions for the amplitudes require the eigenvectors and then application of the initial conditions. The initial conditions are calculated from the deviation from the equilibrium values of the extents of reaction ($\Delta\epsilon$) immediately after the temperature jump (Castellan, 1963); see eq A3 below. Even simple reactions such as these involve algebraically complicated general expressions for the amplitudes; however, by assuming that the relaxation times are sufficiently separated, simplifications are possible. For the case of separated times, we derive expressions for the relative amplitudes in terms of the measured relaxation times (Table II) such that the reaction enthalpies can be determined from linear plots (Figure 4). These plots have the advantage that only quantities that are directly experimentally measurable are used (Jovin, 1975).

Calculating the observed amplitudes for particular models is straightforward matrix algebra, and we only indicate the general steps that are necessary to derive the expressions of Table I using the above assumptions. The two normalized eigenvectors of the matrices in eq A1 and A2 must first be calculated. Note that this involves the eigenvalues and therefore the assumption of separated times. We define the two normalized eigenvectors as Δ^1 and Δ^2. The ith eigenvector is written in terms of its components as $\Delta^i = (\Delta_1^i, \Delta_2^i)^T$. The superscript T refers to the transpose of the vector. The vector of the initial total overall deviation of the extent of reaction from the equilibrium value is given by (Castellan, 1963)

$$\Delta\epsilon^{Tot} = [V\Delta T/(RT^2)]\mathbf{g}^{-1}\Delta\mathbf{H}° \qquad \text{(A3)}$$

where V = volume, ΔT = temperature change, R = universal gas constant, $\Delta\mathbf{H}°$ = vector of the reaction enthalpies with components $\Delta H°_i$ for the ith reaction, and $\mathbf{g}^{-1}$ = inverse of the g matrix (Castellan, 1963), which relates $\Delta\epsilon^{Tot}$ to the vector of the change in the natural logarithm of the association constants due to the temperature jump ($\Delta \ln \mathbf{K}$)

$$\Delta \ln \mathbf{K} = (1/V)\mathbf{g}\Delta\epsilon^{Tot}$$

$\Delta\epsilon^{Tot}$ can be decomposed into the two normal modes, and these are proportional to the eigenvectors

$$\Delta\epsilon^{Tot} = \Delta\epsilon^1 + \Delta\epsilon^2 = \alpha\Delta^1 + \beta\Delta^2 \quad (A4)$$

These simultaneous equations are now solved for α and β in terms of the thermodynamic parameters of eq A3. For the extent of reaction for the first normal mode (fastest relaxation, $\Delta\epsilon^1$), we need only α, since we have assumed that the two reactions are temporally separated, $\Delta^1 = (1, 0)^T$. The general expression valid for both models is then simply

$$\alpha = \Delta\epsilon_1^{Tot} - \Delta\epsilon_2^{Tot}(\Delta_1^2/\Delta_2^2) \quad (A5)$$

Note that the $\Delta\epsilon_i^{Tot}$ values are calculated only from the equilibrium parameters and are independent of the kinetic approximations. The values are then calculated from the eigenvector expressions and eq A3 for the two different models.

Now it is easy to calculate the amplitude of the fastest relaxation. We define the vector of the signal change for 1-mol change of the extent of reaction to be $\Delta\phi$ with components for the ith reaction, $\Delta\phi_i$. Then, the observed amplitude for the faster relaxation (ΔP_1) is

$$\Delta P_1 = (1/V)(\Delta\epsilon^1)^T\Delta\phi = (\alpha/V)(\Delta^1)^T\Delta\phi = (\alpha/V)\Delta\phi_1 \quad (A6)$$

The last equality is due to the assumption of separated reaction velocities, i.e., $\Delta^1 = (1, 0)^T$. In our case, $\Delta\phi_1/V$ is the fluorescence of the ligand per molar solution, since we assume complete quenching and only observe the fluorescence of the ligand.

Substituting α for the two models into eq A6 and writing out the expressions for P_O and P_M of Table II in terms of the concentrations of the chemical species, $\Delta\phi$, and the association constants, we arrive at the expressions in Table II for $\Delta P_1/(P_O - P_M)$, where use has been made of the expression $\tau_1^{-1} = k_1(\bar{P} + \bar{L}) + k_{-1}$. The expression for $\Delta P_{Tot}/(P_O - P_M)$ is easily derived from eq A3 and $(\tau_1\tau_2)^{-1}$ from Table II. General expressions for relative amplitudes, from which those above can be derived, will be published elsewhere.

Registry No. MeUmb-GlcNAc, 37067-30-4; MeUmb$(GlcNAc)_2$, 53643-12-2; MeUmb$(GlcNAc)_3$, 53643-13-3.

References

Allen, A. K., Neuberger, A., & Sharon, N. (1973) *Biochem. J. 131*, 155–162.

Avery, L. (1982) *J. Chem. Phys. 76*, 3242–3248.

Bhavanandan, V. P., & Katlic, A. W. (1979) *J. Biol. Chem. 254*, 4000–4008.

Burger, M. M., & Goldberg, A. R. (1967) *Proc. Natl. Acad. Sci. U.S.A. 57*, 359–366.

Castellan, G. W. (1963) *Ber. Bunsenges. Phys. Chem. 67*, 898–908.

Clegg, R. M., Loontiens, F. G., Van Landschoot, A., & Jovin, T. M. (1976) *International Congress on Biochemistry, 10th*, Hamburg, West Germany, July 25–31, Abstr. 04-2-366.

Clegg, R. M., Loontiens, F. G., & Jovin, T. M. (1977) *Biochemistry 16*, 167–175.

Clegg, R. M., Loontiens, F. G., Van Landschoot, A., Sharon, N., DeBruyne, C. K., & Jovin, T. M. (1980) *Arch. Int. Physiol. Biochim. 88*, B69–B70.

Clegg, R. M., Loontiens, F. G., Van Landschoot, A., & Jovin, T. M. (1981) *Biochemistry 20*, 4687–4692.

Delmotte, F., Privat, J. P., & Monsigny, M. (1975) *Carbohydr. Res. 40*, 353–364.

Jovin, T. M. (1975) in *Concepts in Biochemical Fluorescence* (Chen, R., & Edelhoch, H., Eds.) p 305, Marcel Dekker, New York.

Lis, H., & Sharon, N. (1977) *Antigens 4*, 429–529.

Loontiens, F. G., Clegg, R. M., & Jovin, T. M. (1977a) *Biochemistry 16*, 159–166.

Loontiens, F. G., Clegg, R. M., Van Landschoot, A., & Jovin, T. M. (1977b) *Eur. J. Biochem. 78*, 465–469.

Lotan, R., & Sharon, N. (1973) *Biochem. Biophys. Res. Commun. 55*, 1340–1346.

Monsigny, M., Delmotte, F., & Hêlène, C. (1978) *Proc. Natl. Acad. Sci. U.S.A. 75*, 1324–1328.

Nagata, Y., & Burger, M. M. (1974) *J. Biol. Chem. 249*, 3116–3122.

Privat, J. P., Delmotte, F., & Monsigny, M. (1974a) *FEBS Lett. 46*, 224–228.

Privat, J. P., Delmotte, F., & Monsigny, M. (1974b) *FEBS Lett. 46*, 229–232.

Privat, J. P., Delmotte, F., Mialonier, G., Bouchard, P., & Monsigny, M. (1974c) *Eur. J. Biochem. 47*, 5–14.

Rice, R. H., & Etzler, M. E. (1975) *Biochemistry 14*, 4093–4099.

Rigler, R., Rabl, C. R., & Jovin, T. M. (1974) *Rev. Sci. Instrum. 45*, 580–588.

Thomas, M. W., Walborg, E. F., Jr., & Jirgensons, B. (1977) *Arch. Biochem. Biophys. 178*, 625–630.

Van Landschoot, A., Loontiens, F. G., Clegg, R. M., Sharon, N., & DeBruyne, C. K. (1977) *Eur. J. Biochem. 79*, 275–283.

Van Landschoot, A., Loontiens, F. G., & DeBruyne, C. K. (1978) *Eur. J. Biochem. 83*, 277–285.

Van Landschoot, A., Loontiens, F. G., Clegg, R. M., & Jovin, T. M. (1980) *Eur. J. Biochem. 103*, 313–321.

Viale, R. O. (1971) *J. Theor. Biol. 31*, 501–507.

Wright, C. S. (1977) *J. Mol. Biol. 111*, 439–457.

Wright, C. S. (1980) *J. Mol. Biol. 141*, 267–291.